Title
Thermal Neutron Computed Tomography of Soil Water and Plant Roots

Authors
Leanne G. Tumlinson
Hungyuan Liu
Wendy K. Silk
et al.

Publication Date
2007-08-14

Peer reviewed

Thermal Neutron Computed Tomography of Soil Water and Plant Roots

Leanne G. Tumlinson
716 W. 16th Ave.
Spokane, WA 99203

Hungyuan Liu
McClellan Nuclear Radiation Center
5335 Price Avenue
Bldg. 258
McClellan, CA 95652

Wendy K. Silk
Dep. of Land, Air, and Water Resources
Univ. of California
Davis, CA 95616

Jan W. Hopmans*
Dep. of Land, Air, and Water Resources
Univ. of California
Davis, CA 95616

Neutron radiography is a noninvasive imaging technique that measures the attenuation of thermal neutrons, as is done with x-ray and γ-ray radiography, to characterize the internal composition of materials. Neutron and x-ray imaging are complementary techniques, with neutron imaging especially well suited for materials containing H atoms and other low-atomic-weight attenuating materials. Although neutron computed tomography (NCT) techniques are routinely used in engineering, relatively little is known about their application to soils. We developed new techniques that use thermal neutron attenuation to measure the spatial and temporal distribution of water in soils and near roots at near 0.5-mm spatial resolution or higher. The neutron source was a Mark II Triga Reactor at McClellan Nuclear Radiation Center in Sacramento, CA. After calibration using both deuterated and regular water, the effects of beam hardening and neutron scattering could be corrected for, provided that the total path length for a soil–water mixture does not exceed 1.0 cm, limiting soil sample thickness to about 2.5 cm. Using regular water, for a wide range of soil water content values, experiments demonstrated that NCT is sensitive to small changes in soil volumetric water content, allowing estimation of the spatial distribution of soil water, roots, and root water uptake. Although the spatial resolution of the applied NCT system was 80 μm, an error analysis showed that the averaging measurement volume should be not less than about 0.5 mm for the uncertainty in volumetric water content to be minimized to near 0.01 m^3 m^{-3}. A single root water uptake experiment with a corn (*Zea mays* L.) seedling demonstrated the successful application of NCT, with images showing spatially variable soil water content gradients in the rhizosphere and bulk soil.

Abbreviations: CCD, charge-coupled device; CT, computed tomography; MNRC, McClellan Nuclear Radiation Center; NCT, neutron computed tomography.

Innovative techniques are currently available for nondestructive transient measurement of the plant root system, including root growth, water uptake, and nutrient extraction (Asseng et al., 2000). During the past 15 yr, x-ray computed tomography (CT) measurements have successfully been used to measure soil properties such as bulk density, porosity, water content (Hopmans et al., 1992; Anderson and Hopmans, 1994; Wildenschild et al., 2005), soil structure (Phogat and Aylmore, 1999), and solute concentration (Clausnitzer and Hopmans, 2000). Hainsworth and Aylmore (1986) calculated water flow to a single root using measurements of soil water content with time from wetting to drying for high and low transpiration rates. Heeraman et al. (1997) were the first to image the three-dimensional architecture of a bean root at a spatial resolution <1 mm. Pierret et al. (2003) suggested two-dimensional x-ray CT for higher spatial resolution purposes, to analyze water content depletion around a single root with a resolution of ~250 μm. Thermal neutron radiography and NCT are similar to x-rays, but measure the attenuation of thermal neutrons in imaged objects, recording the attenuated beam as an image by a charge-coupled device (CCD) camera. Neutron imaging works especially well for substances that contain H atoms or other low atomic mass, neutron attenuating materials.

Although neutron attenuation techniques have been used routinely in engineering, relatively little is known about their application to soils. Recent exceptions are the works by Solymar et al. (2003) and Deinert et al. (2004), demonstrating NCT application to estimate spatial distribution of water content in rock and soil, respectively. Some studies have also demonstrated the potential application of neutron radiography to study root water depletion zones and ion uptake mechanisms (Korosi et al., 1999; Furukawa et al., 1999). The most recent study was done by Hassanein (2006), presenting various correction methods for thermal neutron tomography applications to account for backscattering and beam hardening. Preliminary data showed that the current McClellan Nuclear Radiation Center (MNRC) facility can be used to image soil water content and root water depletion using deuterated water, as it is much less attenuating than regular water (Garber and Kinsey, 1976).

In their recent review of root water and nutrient uptake modeling, Hopmans and Bristow (2002) concluded that progress in the basic understanding of transport processes in the plant–soil environment has been slow, specifically regarding interfacial fluxes at the root–soil interface. They speculated that the so-called "knowledge gap" of plant responses to water

Soil Sci. Soc. Am. J. 72:1234-1242
doi:10.2136/sssaj2007.0302
Received 14 Aug. 2007.
*Corresponding author (jwhopmans@ucdavis.edu).

and nutrient limitations is caused by the historical neglect of studies of belowground processes. Mostly, this is caused by the lack of scale-appropriate measurement techniques that would allow estimation of relevant properties and parameters at the spatial scale of about 1 mm. Traditional methods for studying root systems are destructive, tedious, and difficult to interpret. Example methods include excavation, glass-walled rhizotrons, and in situ placement of glass tubes in soils to measure root development using an optical fiber system. Disadvantages of these methods include the destruction of the root system under study and their limited representativeness.

The complex relationship between a root and the surrounding soil has also been explored through elaborate numerical models, including those developed to simulate three-dimensional water and solute transport, water and solute uptake by roots, root growth, and the simultaneous relationships among these processes (Silk and Wagner, 1980; Clausnitzer and Hopmans, 1994; Somma et al., 1998; Vrugt et al., 2001). The experimental data on water flow in corn roots and root system modeling of Doussan et al. (1998a,b) have shown that although water availability in the rhizosphere may be homogenous along primary and lateral roots, water uptake is typically highly heterogeneous.

The general objective of this study was to determine whether the MNRC facility of the University of California, Davis, with its recently upgraded detection system, can be used to measure spatial and temporal changes in volumetric soil water content and root distribution by thermal NCT imaging. The specific objectives were (i) to evaluate the sensitivity of the thermal NCT to soil water content using mixtures of regular and deuterated water (D_2O) by careful calibration and analysis of both the old and upgraded imaging and detection system, and (ii) to explore neutron attenuation methods for estimation of the spatial distribution of root water uptake.

THEORY

Neutron radiography is a noninvasive imaging technique that measures the attenuation of thermal neutrons, much like photons in x-ray and γ-ray radiography, to characterize the internal composition of materials. In both cases, the attenuated beam is recorded as an image by a CCD camera. Neutron imaging works especially well for substances that contain H atoms or other neutron-attenuating materials. Neutron attenuation is complementary to x-rays, as photons are mostly attenuated by high atomic number materials. Neutron scatter and absorption are attenuative processes where the neutron strikes and is deflected or absorbed, respectively, by the target nucleus (Lamarsh, 1983, p. 44–86). In analogy to photon attenuation by scattering or absorption (x- and γ-rays), neutron attenuation is described by Beer's law, relating a beam of approximately mono-energetic neutrons with an incident intensity I_o [no. of incident neutron L^{-2} T^{-1}], which penetrates a material of thickness x [L] and effective macroscopic cross-section Σ [L^{-1}], to yield a reduced intensity, I, at the detector screen, or

$$\frac{I}{I_o}=\exp(-\Sigma x) \qquad [1]$$

where the coefficient Σ is defined by the product of atom density, N [no. of atoms L^{-3}], and nucleus cross-section, σ [L^2], or

$$\Sigma = N\sigma \qquad [2]$$

and N is defined by material density, ρ, divided by the atomic weight of the material, M (Lamarsh, 1983, p. 44–86). More clearly, Σ defines the probability of neutron interaction per unit path length of material. Typically, σ is expressed in barns, with 1 barn = 10^{-24} cm^2, with numerical values listed for a wide range of isotopes in Garber and Kinsey (1976). Both σ and Σ are a function of neutron energy or the energy spectrum of the neutron beam. Using notation typically used in x-ray attenuation (Clausnitzer and Hopmans, 2000), Σ is replaced by μ, defined as the probability that a photon is removed from the beam per unit path length [L^{-1}]. The mean free path length of the neutron, λ, is determined from the attenuation coefficient, or $\lambda = 1/\Sigma$. As the effective cross-sectional area of protons is large for thermal neutrons, in concept, neutron radiography would be well suited for the measurement of water distribution in soils.

Rewriting Eq. [1] yields

$$\ln\frac{I_o}{I}=\Sigma x=\sum_{i=1}^{n}\Sigma_i x_i \qquad [3]$$

where the right-hand side is decomposed by including the attenuation of each separate component i. When using aluminum blocks (subscript al) with cylindrical holes filled with material (subscript m) of silica beads (SiO_2), Oso Flaco sand, H_2O, or D_2O, Eq. [3] is written as

$$\ln\frac{I_o}{I}=\Sigma_m x_m+\Sigma_{al}x_{al}$$

yielding

$$\ln\frac{I_o}{I}-\Sigma_{al}x_{al}=\Sigma_m x_m \qquad [4]$$

Assuming that Beer's law applies, a plot of the left-hand side of Eq. [4] vs. x_m must yield a linear relationship, with the slope of the line equal to Σ_m, representing the constant attenuation coefficient and x_m denoting the variable path length of material i. Moreover, since I and I_o are equal when x_m is zero, the regression line must go through the origin. Nonlinearity usually indicates beam hardening and neutron backscatter, both phenomena resulting in a decrease of the attenuation coefficient with increasing sample thickness. In addition, there can be a background scattering contribution as a result of detecting neutrons that have backscattered to the screen from interactions with the experimental surroundings and have no relation to sample attenuation.

Beam hardening typically occurs if the neutron beam is polychromatic, resulting in differential attenuation due to absorption along the path length of the imaged object as it transverses the object, with lower energy neutrons removed first. The assumption of Eq. [1] and [2] is that all detected neutrons do interact with the sample material by the scintillation screen, with reduction in I_o caused by single interactions. There are complications, however. For example, the attenuation of neutrons by water is primarily due to scatter (Lamarsh, 1983, p. 44–86). Because the theoretical mean free path of thermal neutrons in regular water is about 3 mm, a sample thickness >3 mm is expected to result in multiple interactions of scattered neutrons. The multiple scattering effect significantly reduces Σ_m of water from its theoretical value due to an overestimation of the transmitted neutron flux, I.

Rewriting Eq. [4] to allow for a mixture of silica or sand with water yields

$$\ln\frac{I_o}{I}=(1-\phi)\Sigma_s x_{pm}+\theta\Sigma_l x_{pm}+(\phi-\theta)\Sigma_a x_{pm}+\Sigma_{al}x_{al} \qquad [5]$$

where Σ_s, Σ_l, and Σ_a are the macroscopic cross-sections of the solid, liquid, and air phases of the porous sample, respectively. The length of the total porous medium is represented by x_{pm}, and ϕ and θ correspond to porosity (m^3 pores m^{-3} soil) and volumetric water content (m^3 water m^{-3} soil), respectively (Wildenschild et al., 2002). It is reasonable to assume that the contribution of Σ_a to Σ_{pm} is negligible, so Eq. [5] can be reduced to

$$\ln\frac{I_o}{I}=(1-\phi)\Sigma_s x_{pm}+\theta\Sigma_l x_{pm}+\Sigma_{al}x_{al} \quad [6]$$

For calibration purposes, to determine soil water content from neutron attenuation, Eq. [6] was normalized, using

$$\frac{\ln\frac{I_o}{I}-(\Sigma x)_{al}}{x_{pm}}=\Sigma_{pm} \quad [7]$$

where x_{pm} denotes the thickness of the soil sample, yielding

$$\Sigma_{pm}=(1-\phi)\Sigma_s+\theta\Sigma_l \quad [8]$$

With all terms of Eq. [7] either known or measured, the soil's volumetric water content can be estimated from this linear relationship, noting that Σ_l is the slope and $(1-\phi)\Sigma_s$ is the intercept.

MATERIALS AND METHODS

Facility

The study was conducted at the 2-MW Mark II TRIGA research reactor of the University of California, at McClellan in Sacramento, CA (Wilding et al., 2005). The core of the reactor consists of 100 stainless steel 56-cm (22-inch) fuel rods, containing a mixture of U (20% enriched ^{235}U) and ZrH_2. The middle 38-cm (15-inch) portion of each rod holds a U and ZrH_2 mixture and is capped on either end by 9 cm (3.5 inches) of graphite to prevent neutron leakage. A 26.5-m^3 (7000-gallon) tank filled with high-purity water surrounds the core. To maintain a water temperature in the tank surrounding the reactor core at 110°F, water is circulated at a rate of 3.8 m^3 min^{-1} (1000 gpm) after cooling to 90°F.

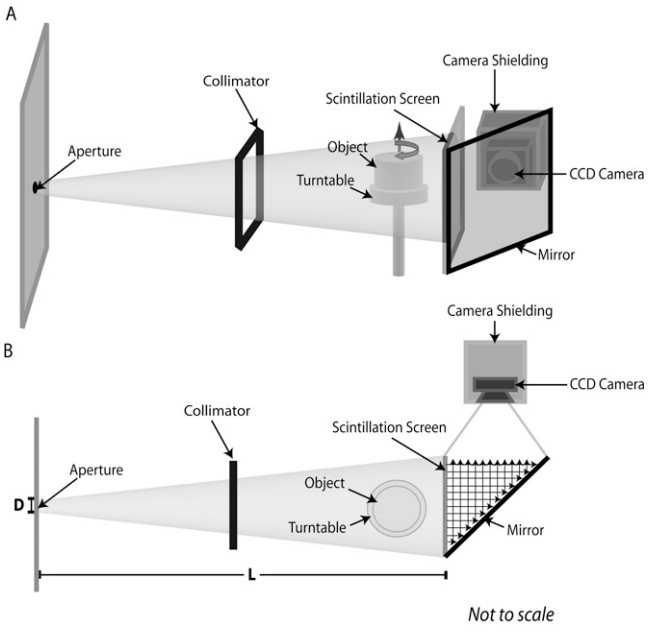

Fig. 1. (A) Three dimensional and (B) plan view of the tomography system in Bay 3 at the McClellan Nuclear Radiation Center (D is aperture width and L is distance between aperture and screen).

The neutron source in the core of the reactor consists of a rod with a mixture of Be (10% by weight ^9Be) and ^{241}Am (Research Reactor Safety Analysis Services, 1991). Uranium-235, being a fissile material, absorbs neutrons of any energy level, especially those with thermal energies, thereby causing nuclear fission (Lilley, 2001). After absorption by a ^{235}U nucleus, a compound nucleus is formed ($^{236*}U$), which on excitement splits into two lighter fragments and two to four neutrons. The neutrons induce fission of other ^{235}U nuclei, resulting in sustained fission. This nuclear reaction is moderated by ZrH_2 in the fuel rods, in addition to the light water surrounding the core, and is controlled by six control rods including the transient rod. The transient rod includes boron carbide (B_4C) and can be removed from the core instantly to boost neutron production. Five control rods can be inserted into the core to decrease neutron production, as B has a much higher absorption cross-section than light water. A total of four beam tubes filled with He gas allow thermal neutrons emitted from the core to enter four different experimental bays, with In–Cd collimators absorbing divergent neutrons. All our experiments were conducted in Bay 3, which has a thermal neutron flux of 1.2×10^7 neutrons cm^{-2} s^{-1}, comprising about 50% of the total beam flux at the sample location (Gibbons and Shields, 1998).

Imaging Equipment

The tomography system consists of the neutron source, a sample turntable, a ^6Li scintillation screen that is sensitive to thermal neutrons (<1.0 eV), a mirror, a CCD camera, and a computer with acquisition software (Fig. 1). The camera is shielded from gamma rays and scattered neutrons by Pb and lithiated (>90% enriched ^6Li) polyethylene encasements, respectively. Although initial experiments were conducted with an old imaging system, the presented results were obtained using an upgraded system, including a new CCD camera, translation stage, rotation stage, mirror, and scintillation screen (VanDalen et al., 2005). The upgraded camera is an Apogee-ALTA camera equipped with a CCD chip with a 2048 by 2048 array of 13-μm pixels. The camera was mounted on a translation stage, allowing the user to change the object size by moving the camera along its optical axis. The upgraded system included a turntable allowing rotational increments of 0.001° during CT image acquisition. Enhancements included a new mirror and thicker screen, thereby allowing absorption of a wider range of neutron energies, including epithermal neutrons at slighter higher energies than thermal neutrons. The new mirror consisted of float glass and was coated with enhanced aluminum yielding >90% reflection of the visible wavelength range into the CCD camera. The upgraded CT system improved spatial resolution to about 80 μm.

The neutron beam entering the bay through the aperture contains many divergent neutrons. As the neutron beam travels farther away from the aperture, an increasing number of divergent neutrons will move out of the beam line, thereby creating a parallel incident beam. A lithiated polyethylene collimator is installed in the beam line to further absorb divergent neutrons before they can interact with the object or scintillation screen. With an aperture width (D) of 2.8 cm and aperture distance to the screen (L) of 653 cm, the L/D radio is 233 (Fig. 1), which is relatively high. The large L/D ratio reduces noise and increases spatial resolution (Schillinger et al., 2000; Koerner et al., 2001), as it decreases the likelihood of divergent neutrons reaching the object or scintillation screen, thereby increasingly satisfying the

required parallel neutron beam assumption. The beam has a diameter of 50 cm at the scintillation screen. Through a mirror, the emitted light of the scintillation screen is reflected toward the CCD camera and is recorded as a 16-bit gray-scale digitization (Koerner et al., 2001). Since relative light intensity varies with the degree of neutron attenuation, the CT method can be used to infer sample material composition.

Using CT, a complete image consists of a series of 360 radiographs collected by rotating the scanned object on the turntable in 0.5° steps from 0 to 180°. A radiograph is collected at each step. The exposure time for each tomograph was 20 s, thus requiring a total of about 2 to 3 h to obtain a complete CT scan with a voxel size of 80 μm. The raw images were preprocessed by correcting for background noise and beam fluctuations and were normalized by the flat field image. Computer reconstruction of the radiographs was accomplished using a filtered back-projection algorithm (Richards et al., 2004) that uses the Fourier slice theorem of Kak and Slaney (2001, p. 60–75). Imgrec, the software used to acquire, process, and reconstruct the CT data, was developed at Lawrence Livermore National Laboratory (University of California, Livermore) by Dan Schneberk (DanSchneberk@llnl.gov). In the final preprocessing stage, Slicer 3D (Fortner Research, 1996) was used to visualize the data, and Python programming allowed volume averaging of the reconstructed data.

Experiments

A sequence of experiments was conducted to evaluate the potential application of thermal NCT in soils. The first set of experiments (Exp. A) were designed to evaluate the effects of sample thickness on beam hardening and scattering of the incident beam, using both regular (H_2O) and deuterated (D_2O) water and their mixtures, silica beads (SiO_2), and Oso Flaco sand as porous media. The second set of experiments (Exp. B) were conducted to determine calibration curves, relating volumetric water content (θ) to the attenuation coefficient, Σ_{pm},, of a silica bead or Oso Flaco sand with D_2O, H_2O, or a blend of the two waters, and to evaluate measurement uncertainty. The final experiments (Exp. C) used the calibration curve to determine the spatial distribution of water in a sandy soil and around a growing corn root.

For Exp. A and B, the irradiated sample holder consisted of a 3-cm-tall, 7- by 7-cm square aluminum block with 5.0-mm-diameter machined circular holes arranged in a 10 by 10 pattern, for a total of 100 holes. A variable number of holes were filled with either 99.9% pure D_2O (CDN Isotopes, Pointe-Claire, QB, Canada), regular water, silica beads, Oso Flaco sand, or mixtures of water (both regular and deuterated) with the sand or silica beads. Figure 2a shows a plan and three-dimensional view of the sample holder, where a variable number of holes in the direction of the neutron beam (black arrow) are filled with material (*m* or *pm*). Uniform water content values were obtained by mixing a known mass of sand with a known volume of water to achieve the desired water content. The silica beads were consistently packed to a bulk density of 1.51 g cm^{-3}. The Oso Flaco fine sand was packed at an approximate bulk density of 1.25 g cm^{-3} (Tuli and Hopmans, 2004). Depending on the experiment, radiographs were obtained at 0, 90, or 180° object rotations. Except for Exp. C, average *I* values were calculated by taking the average of a vertical transect in the center of each column of the sample holder in the radiograph. The I_o values corresponding with the *I* values of the radiographs were determined similarly from the flat image (no sample). Initial experiments were conducted with an outdated CCD camera and defective scintillation screen. The results presented here were obtained with an upgraded system allowing increased spatial resolution and improved uniform detection by the new scintillation screen.

Experiment A: Beam Hardening and Backscattering

A variable number of holes across the 10 columns of the aluminum sample holder (Fig. 2b) were filled with Oso Flaco sand and SiO_2 beads, to achieve a range of porous material thicknesses. For example, filling eight of the 10 5-mm holes with sand resulted in a total path length, x_m, of 4 cm. Additional experiments were conducted to determine the validity of Eq. [1] for a range of blends of D_2O with H_2O, including pure D_2O and regular H_2O, using aluminum blocks of both 2.5- and 5.0-mm-diameter holes.

Experiment B: Calibration and Error Analysis

A set of calibration experiments was performed to determine the regression coefficients of the relationships between volumetric water content and neutron beam attenuation. For that purpose, a variable number of holes were filled with silica beads or sand, pure D_2O or H_2O, or a 50:50 blend of porous material and water, to achieve a range of water content values, with volumetric water content determined by the ratio of water path length (number of water-filled holes times 0.5 cm) to total path length (5 cm) across each column of the

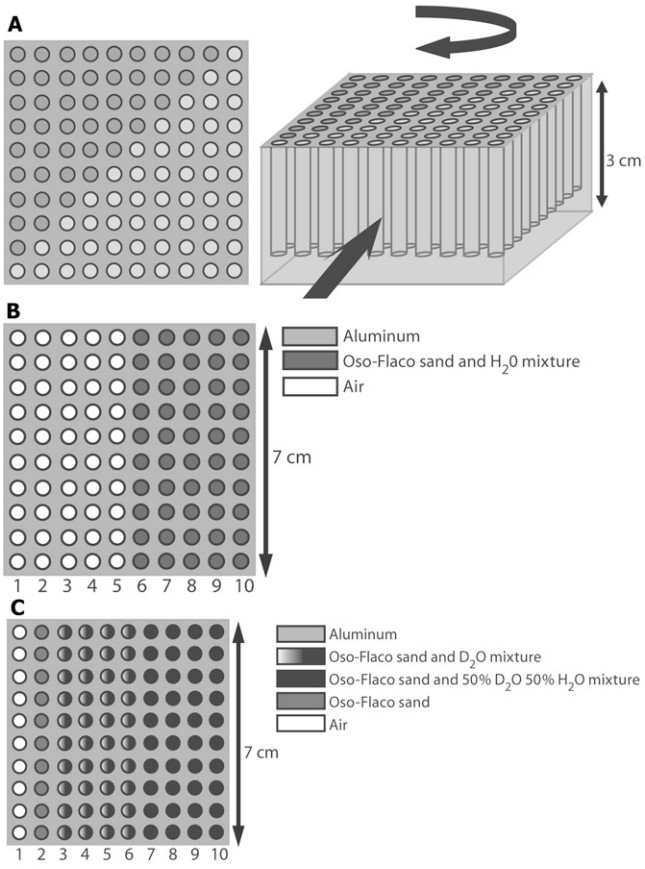

Fig. 2. (a) Plan and three-dimensional view of aluminum sample holder with Column 1 through 10 in the direction of the incident neutron beam (straight arrow) and the curved arrow indicating the direction of rotation; (b) with Oso Flaco sand and mixtures of Oso Flaco sand with 100% D_2O and 50:50 D_2O/H_2O mixture with volumetric water content range between 0.10 and 0.46 m^3 m^{-3}; and (c) with five columns of Oso Flaco sand and 100% H_2O mixtures for volumetric water content values ranging between 0.00 and 0.14 m^3 m^{-3}.

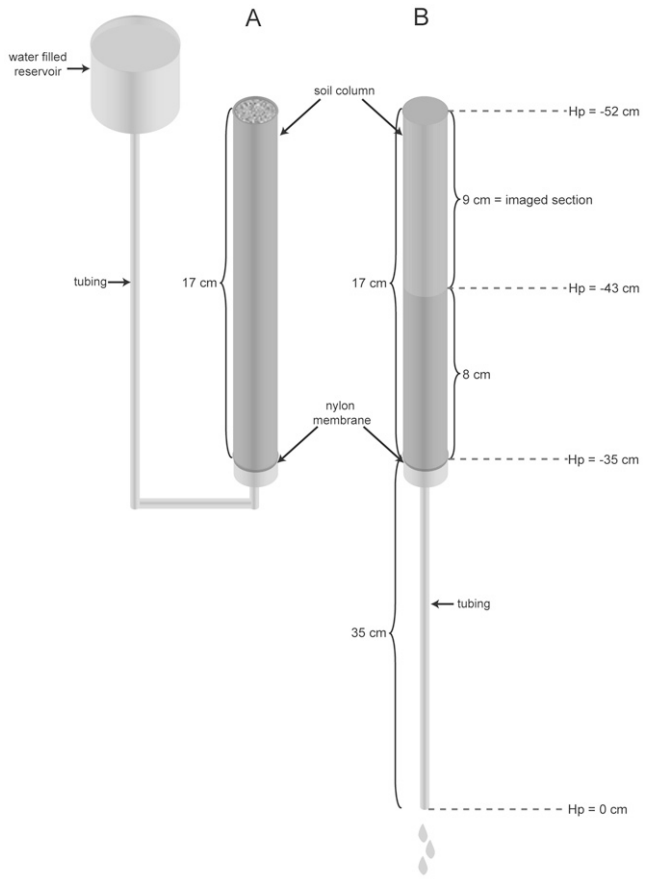

Fig. 3. Diagram of cylinder experiment showing (A) wetting and (B) draining configuration (H_p is matric pressure head).

sample holder. For an additional calibration experiment, all 10 holes of each column of the sample holder were filled with wetted sand after the sand was mixed with predetermined and variable amounts of deuterated water and the 50:50 blend to achieve a water content range between 0.14 and 0.46 $m^3\ m^{-3}$. In a final calibration experiment, five sets of 10 holes were filled with the Oso Flaco sand with predetermined amounts of H_2O in the volumetric water content range between 0.00 and 0.14 $m^3\ m^{-3}$ (Fig. 2c). Radiographs for these experiments were taken at 0° of rotation only.

The reconstructed images of the calibration experiments were also used to conduct an error analysis by extracting voxel attenuation values from the stacked slices for Columns 6 through 10 of Fig. 2c. Average attenuation values as a function of averaging volume were obtained for the range between 0.08 by 0.8 by 0.8 mm or 80 by 80 by 80 μm, equal to voxel size, and 2.00 by 2.00 by 2.00 mm. With the center of each averaging volume equal and independent of changing size (L), the averaged volume was increased from 1 by 1 by 1 voxel to 25 by 25 by 25 voxels.

Experiment C: Applications

Oso Flaco sand was packed to a bulk density of 1.44 g cm^{-3} in a 17-cm-long aluminum cylinder with an inner diameter of 2.3 cm. The sand was supported by a nylon membrane filter with 1.2-μm pore size at the bottom end of the cylinder (Fig. 3A). The soil column was wetted in steps to saturation by elevating a water-filled reservoir, thereby applying a constant water pressure at the bottom of the column for each step. All tube connections were sealed to omit air entry into the system. Once the column was fully saturated, the top of the column was covered and a constant suction of –35 cm was applied to the bottom using a hanging water column (Fig. 3B). The column was allowed to drain for 2 h before the hanging water column was removed, at which time the column was sealed at the bottom. The matric head (H_p) of the imaged section ranged from –35 cm at the bottom to –52 cm at the top after hydraulic equilibrium was attained. The column was refrigerated upright for 24 h, after which a full CT scan of the top 9 cm was conducted during a 2-h period. Subsequently, the column was sliced into nine 1-cm-thick slices, and volumetric water content was determined after oven drying so that soil water retention curves using the CT and gravimetric data could be compared.

In a second experiment, the Oso Flaco sand was mixed with a predetermined amount of water to achieve a bulk soil water content of about 0.10 $m^3\ m^{-3}$ and packed into the aluminum column. After 3 d of germination, a 1- by 0.8-cm corn seed with a tap root measuring 2.0 cm was planted into the column. The column was covered with a vented piece of Parafilm to prevent evaporation and kept at 20°C. The seed was allowed to grow for 6 d, at which time a full CT scan (lasting 3 h) was taken of the plant. To quantify the spatial variations in soil water content near the root–soil interface, a total of eight horizontal transects was analyzed along two neighboring vertical slices (of 80-μm thickness). After imaging, the plant was extracted intact and measured for root length and thickness. The root system consisted of one 1-mm, single tap root with no laterals, reaching a length of approximately 10 cm, which corresponds to a growth rate of 1.3 cm d^{-1}.

RESULTS

Experiment A: Beam Hardening and Backscattering

By plotting the left-hand side of Eq. [4] vs. x_m for each of the columns in Fig. 2a through 2c, the slope of the line is equal to Σ_m, as Σ_m must be constant across the object for each material. Moreover, since I and I_o are equal when x_m equals zero, the regression line must go through the origin. The results are shown in Fig. 4a for the SiO_2 and Oso Flaco sand, and in Fig. 4b for the various water mixtures. Nonlinearity is an indication of beam hardening or neutron scattering and backscattering from the surroundings.

We found that the Σ_m value of SiO_2 using the old system was more than twice its value of 0.06 cm^{-1} determined using the upgraded system. This inconsistency is probably caused by the increase in scintillation screen thickness and increased sensitivity to neutron scattering by the upgraded system. The thicker screen increases the absorption of the higher energy neutrons, thereby causing lower values of Σ_m. There is little difference between SiO_2 and Oso Flaco sand, as their regression lines have approximately equal slope and intercept values. We note that the measured attenuation value for SiO_2 is significantly smaller than its theoretical value of 0.57 cm^{-1}, as listed in Garber and Kinsey (1976) at 0.025 eV. This is probably caused by the polyenergetic nature of the neutron beam.

The results for the water mixtures in Fig. 4b clearly show that beam hardening and neutron scatter occur for regular water and for the 50:50 and 25:75 D_2O/H_2O mixtures. Only the relationship for pure D_2O (diamond symbol) is linear, with a slope, Σ_m, of 0.27 cm^{-1}. As for the glass beads, the attenuation value is also significantly lower than the theoretical value of 0.65 cm^{-1} for pure D_2O at 0.025 eV. For all mixtures other than pure D_2O, we conclude that water sample thickness should not exceed 1 cm to maintain sensitivity (shaded box in

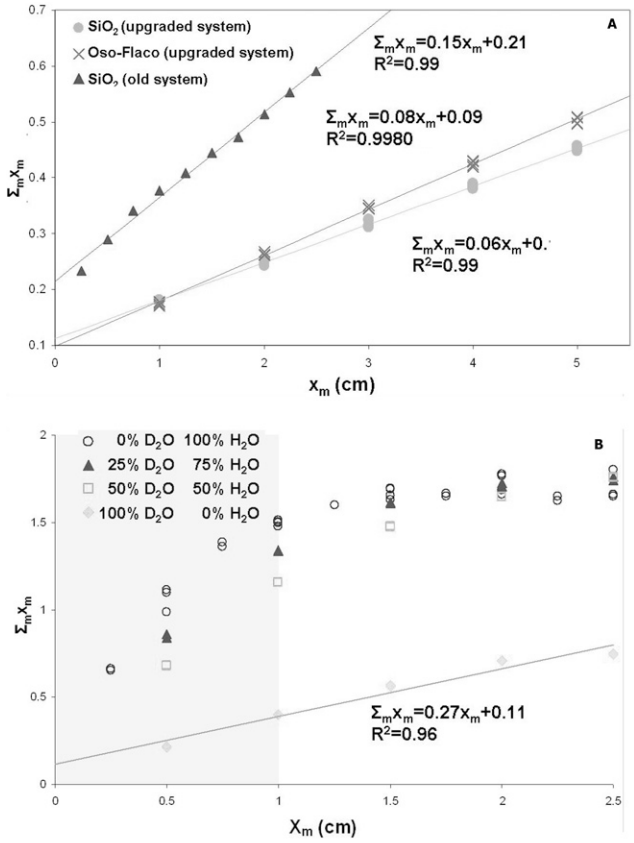

Fig. 4. Beer's law testing (macroscopic cross-section of the porous material $\hat{\Sigma}_{pm}$ vs. material thickness x_m) for (a) SiO_2 and Oso Flaco sand, and (b) H_2O and D_2O mixtures. Shaded box shows range of system sensitivity for regular water.

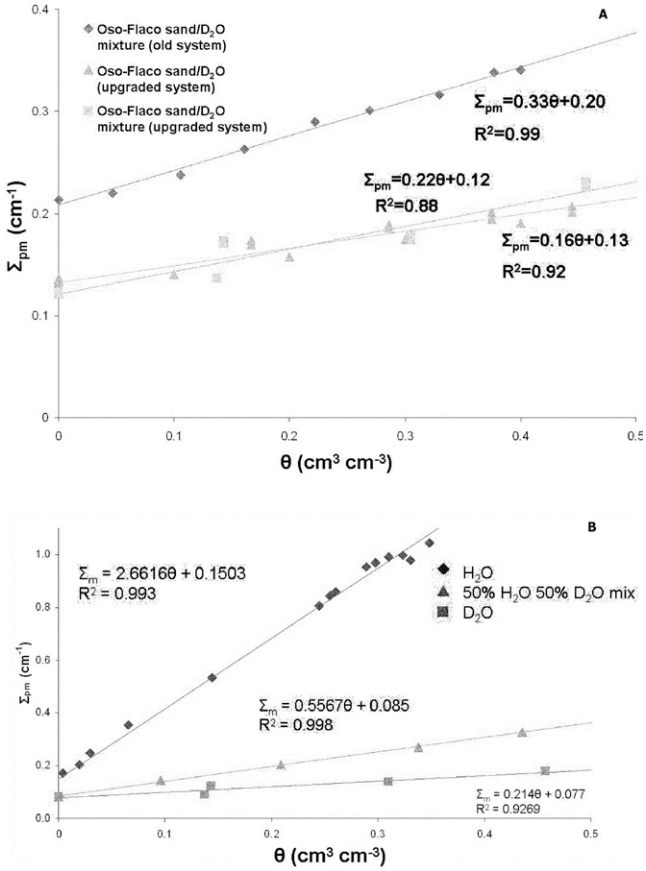

Fig. 5. Calibration curves (macroscopic cross-section of the porous material $\hat{\Sigma}_{pm}$ vs. volumetric water content θ) for (a) Oso Flaco sand and D_2O, with separate phases (triangles) and mixed (squares); and (b) mixtures of Oso Flaco sand and pure H_2O, 100% D_2O, and 50:50 D_2O/H_2O blend.

Fig. 4b). These results clearly demonstrate that significant beam hardening and neutron scatter occur for regular water, due to its higher absorption and scattering cross-section and a corresponding theoretical Σ_m of 3.25 cm^{-1}. Beam hardening and neutron scattering is much less a factor for deuterated water; however, the sensitivity to water content changes is reduced, as is evident by the smaller slope value for the data of 100% D_2O. Similarly, beam hardening does not occur for the silica beads and sand if the sample thickness is 5 cm or less.

Experiment B: Calibration and Error Analysis

For the calibration experiments, results were evaluated using Eq. [8]. Mixtures of Oso Flaco sand and D_2O were prepared with volumetric water content values ranging between 0.00 and 0.44 $m^3\ m^{-3}$. The true water content was determined from oven drying. The calibration data are compared from an experiment whereby similar volumetric water content values as the mixtures were achieved by varying the number of holes filled with sand and D_2O. The resulting calibration curves are presented in Fig. 5a (two bottom lines). Results with the old system are included for comparison (top line). Since the two regression curves are similar, we conclude that calibration curves can be obtained with or without mixing of the water with the porous medium. Moreover, the calibration curves are clearly linear, demonstrating that deuterated water is preferred for larger diameter soil samples (5 cm).

To further test the applicability of regular water for smaller soil samples, Oso Flaco sand was mixed with varying amounts of H_2O to achieve a volumetric water content range between 0.00 and 0.14 $m^3\ m^{-3}$ in an additional calibration experiment. This θ range was chosen so as not to exceed the maximum allowable path length (x_m = 1 cm) of water so that the calibration curve would remain linear. Since the total path length across the aluminum sample holder is 5 cm (10 holes of 0.5-cm diameter each), the maximum allowable θ was 0.20 $m^3\ m^{-3}$. The final calibration curves, including those for pure D_2O and the 50:50 D_2O/H_2O blend are presented in Fig. 5b. The pure water calibration data for θ values >0.2 $m^3\ m^{-3}$ were obtained from the cylinder data of Exp. C. The results show that the sensitivity of neutron attenuation to θ is much greater when using H_2O than D_2O or a mixture of the two. We thus conclude that the best results can be obtained using pure water, rather than adding D_2O, but that the maximum effective path length through water cannot exceed 1.0 cm.

The results of the error analysis are presented in Fig. 6, with the maximum averaging volume size limited by the diameter of the 5-mm hole. The mean Σ_{pm} ($\hat{\Sigma}_{pm}$) value for the pure water as a function of averaged volume is presented in Fig. 6a. Similar analyses (not presented) were obtained for the D_2O and 50:50 D_2O/H_2O blend. As expected, the standard deviation of measurements is inversely related to the size of the averaging volume. It should be noted that there is some bias introduced in these results due to the fact that the sample size decreased with increasing side length (L), from 480 samples

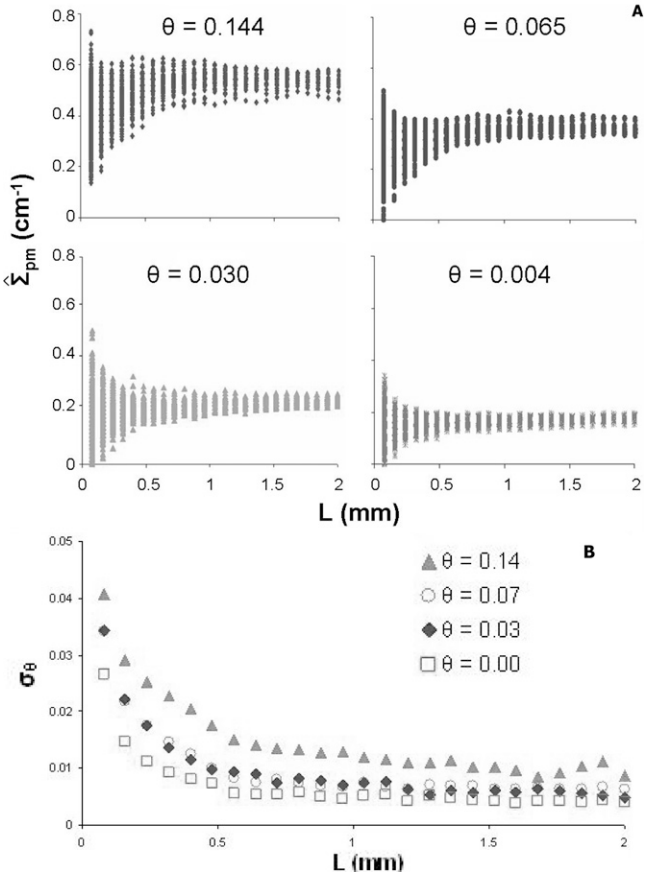

Fig. 6. Plot of (a) the macroscopic cross-section of the porous material, $\hat{\Sigma}_{pm}$, and (b) the standard deviation of the volumetric water content, σ_θ, vs. the side length, *L* (mm), of the averaging volume using pure H_2O.

at L = 80 μm (one voxel), to 90 at L = 0.4 mm, to 40 at L = 0.8 mm, and to 10 samples at L = 2 mm (averaging 25 voxels). The results show that the standard deviation of $\hat{\Sigma}_{pm}$ generally increases as the water content increases, implying that spatial variability increases with θ. This result, however, can also be caused by increased neutron scattering with an increase in θ. Using the calibration curves in Fig. 5b, we calculated the standard deviation of θ (σ_θ) for a given volume side length, and present the results for pure water in Fig. 6b. As expected, σ_θ decreased with increased averaging volume. Moreover, we conclude that measurement uncertainty is minimal for an averaging volume of about 0.5 by 0.5 by 0.5 mm or larger. Though not presented, we found that σ_θ for the D_2O and the 50:50 D_2O/H_2O blend was almost an order of magnitude larger than for the H_2O experiments due to the lower measurement sensitivity of D_2O. We also note that the average 2.00- by 2.00- by 2.00-mm attenuation values are included in the pure water calibration of Fig. 5b.

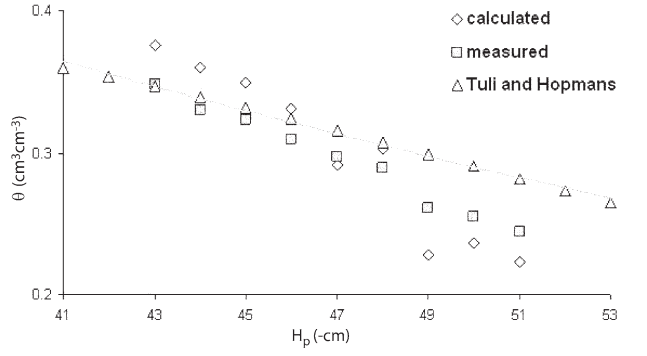

Fig. 7. Soil water retention curve (volumetric water content θ vs. matric pressure head H_p) measured from computed tomography (CT) and gravimetric data from Exp. C. Data from Tuli and Hopmans (2004) included for comparison.

Experiment C: Applications

After reconstructing the three-dimensional volume from the CT measurements of the upper 9 cm of soil in the aluminum cylinder, mean Σ_{pm} values using 2.0- by 2.0- by 2.0-mm averaging volumes were calculated for each 1-cm vertical section. After the CT measurements were completed, the imaged soil was sliced into 1-cm sections and volumetric water content was determined gravimetrically from oven drying. Water content values for the 1-cm sections ranged from 0.22 (top) to 0.38 m^3 m^{-3} (bottom), and corresponded to H_p values of −52 cm (top) and −43 cm (bottom), respectively. Since the column diameter was 2.3 cm and the maximum path length in pure water was determined to be 1 cm (Fig. 4b), the maximum permissible θ is approximately 0.43 m^3 m^{-3}. These data were also included in the calibration curve in Fig. 5b. The soil water retention curves using the gravimetric and CT data are compared in Fig. 7 with the independent retention data of Tuli and Hopmans (2004). Deviations between the CT and gravimetric data are <0.02 m^3 m^{-3}, which is what can be expected from the error analysis. In addition, differences are to be expected because the measurement volume for the gravimetric analysis (5 cm^3) was about 10 times larger than the averaging volume used for the reconstruction of the three-dimensional images (about 0.25 cm^3).

After reconstruction of the CT images, the three-dimensional values of Σ_{pm} were divided into 0.05 cm^{-1} intervals. We found that soil Σ_{pm} values ranged from 0.30 to 0.99 cm^{-1} and root Σ_{pm} values ranged from 1.00 to 3.00 cm^{-1}. Using the water calibration curve of Fig. 5b, these ranges corresponded to θ between 0.08 and 0.32 and between 0.33 and 1.00 m^3 m^{-3} for soil and root, respectively. From gravimetric measurements it was determined that the initial water content before transplanting was 0.12 m^3 m^{-3}. This value was slightly higher than the imaged water content for the 1-cm section below the upper 9.8 cm of the cylinder after 6 d, which was 0.11 m^3 m^{-3}. Thus, it can be concluded that there was little or no water loss from below the top 10 cm of the cylinder with the tap root. From the CT images in Fig. 8a, we were able to compute soil and root water content and their spatial variations. We estimate that total soil water storage decreased 0.76 cm^3 (1.49 mm) and root length increased 8 cm during the 6-d growing period. Using the neutron attenuation measurements, we estimate that total root water volume in the 8-cm root (excluding the seed) was 0.083 cm^3. Therefore, the total water loss by transpiration during the 6-d period was 0.68 cm^3, corresponding to total *water depth* of 1.6 mm. Root length was measured before transplanting and again (using the reconstructed three-dimensional volume) after 6 d of growth. The average root elongation rate was 1.33 cm d^{-1}. Interestingly, this rate is less than half that

reported by Sharp et al. (1988), who found root growth rates between 1.0 and 3.1 mm h^{-1}.

The series of eight analyzed transects are displayed in Fig. 8a. The corresponding water content distributions are presented in Fig. 8b, where the 1-mm-thick root is indicated with the dashed box in each of the plots. We found that the volumetric water content of the bulk soil was highly variable and ranged between 0.10 and 0.20 m^3 m^{-3}. At the low growth rates and transpiration rates of these experiments, the horizontal distribution of rhizosphere water content did not vary appreciably at different distances from the root tip. This implies that plant water uptake is synchronized with soil water diffusion to create a steady pattern of water content around the root. Unexpectedly, CT measurements showed evidence of a transition zone of higher water content between the root surface and surrounding sandy soil. The wet transition zone is visible in the rhizosphere, perhaps 0.5 mm, on both sides of the root and could be an artifact of volume averaging; however, the effect of volume averaging should not extend farther than two or three voxels. Possible explanations include soil wetting by the root or a physical displacement of soil particles relative to water during root penetration of the soil. Another unexpected result was that CT measurements showed that beyond the wet transition zone, the volumetric water content was lower on the right-hand side than on the left-hand side of the root for the two slices shown. This anisotropy might be due to variation in any of several properties: spatial distribution of initial water content caused by packing variations, air entry into soil pores as the root takes up water, or root–soil contact along the root.

SUMMARY AND CONCLUSIONS

Laboratory experiments conducted at the MNRC (University of California-Davis) suggest that thermal NCT can be an excellent means to measure soil water content and plant root water uptake dynamics at a spatial resolution of 0.2 mm or higher. Although initial measurements indicated that deuterated water would need to be used, calibrations with the upgraded detection system clearly showed that regular water is preferred because of the higher sensitivity to neutron attenuation. To eliminate beam hardening and scattering effects, however, the total water path length for soil–water mixtures should not exceed 1.0 cm, thus limiting soil sample diameter to about 2.5 cm. Volume averaging error analysis showed that the optimal averaged volume for Oso Flaco sand with H_2O is about 0.5 by 0.5 by 0.5 mm, with a standard deviation of water content of about 0.01 m^3 m^{-3}. Water retention curves

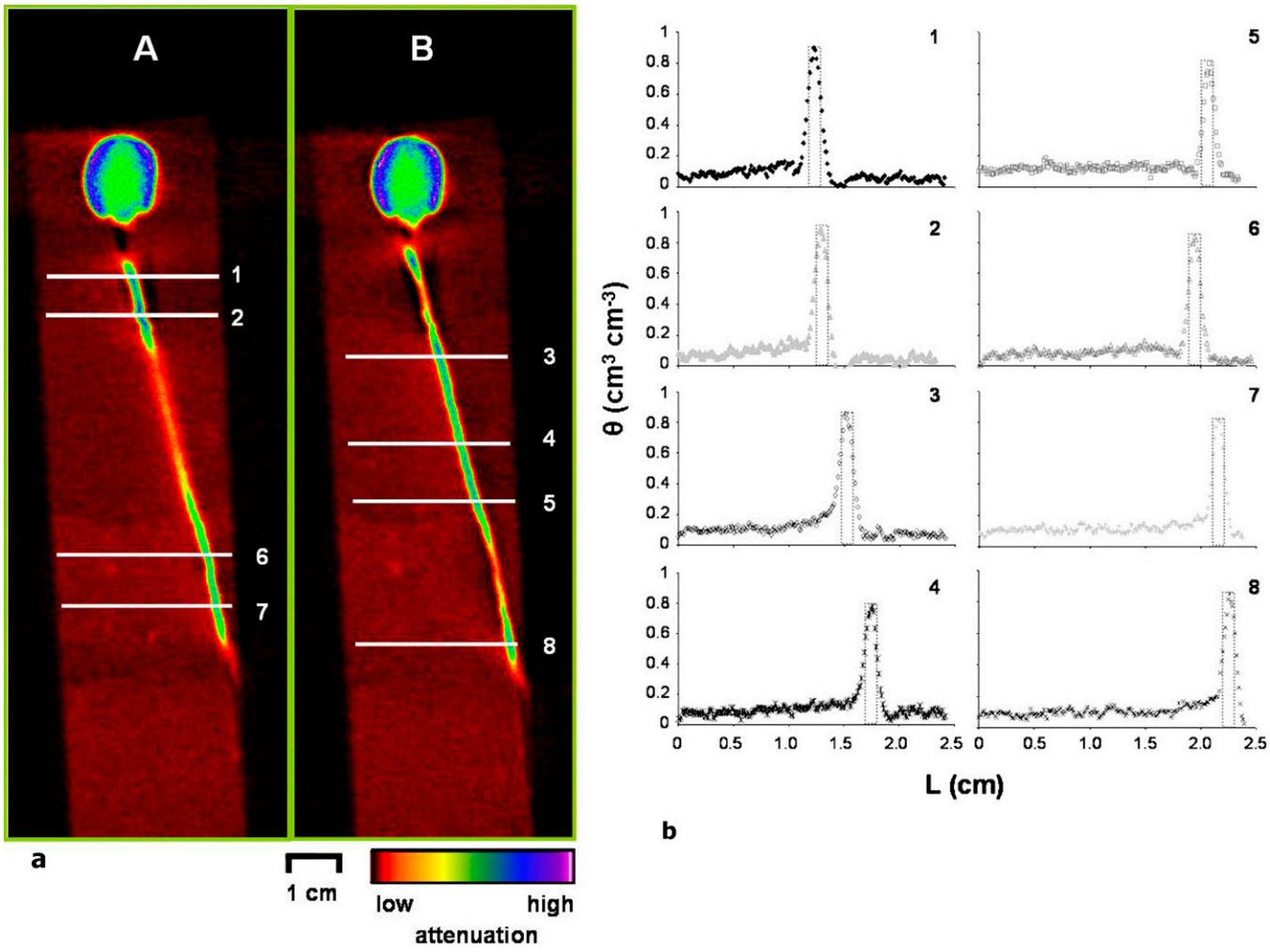

Fig. 8. (a) Two vertical slices of root experiment (A and B) at different positions through the three-dimensional data, showing the location of each transect taken across each image (1–8), and (b) plots of volumetric water content (θ) vs. length (*L*) for Transects 1 through 8. Dashed line box indicates 1-mm root. Transects begin on the left and end on the right of the root.

were successfully obtained using both tomography and gravimetric data for Oso Flaco sand with θ ranging from about 0.22 to 0.38 $m^3\ m^{-3}$. Using the NCT measurements, we also successfully determined the root growth rate (1.33 cm d^{-1}), root water volume (0.083 cm^3), and total water lost by transpiration (0.68 cm^3) of a growing corn root during a 6-d growth period. Experiments on the spatial distribution of root water uptake by a corn root showed the presence of clear soil water content gradients in the rhizosphere, which are worthy of further study to clarify the kinematics of water uptake around the growth zone and developing root tissue.

ACKNOWLEDGMENTS

This project was funded by a grant from the U.S. Dep. of Energy for Innovations in Nuclear Infrastructure and Education (INIE). We especially thank the technical support staff at the McClellan Nuclear Radiation Center of UC-Davis.

REFERENCES

Anderson, S.H., and J.W. Hopmans (ed.). 1994. Tomography of soil water root processes. SSSA Spec. Publ. 36. SSSA, Madison, WI.

Asseng, S., L.A.G. Aylmore, J.S. MacFall, J.W. Hopmans, and P.J. Greogory. 2000. Computer-assisted tomography and magnetic resonance imaging. p. 343–364. *In* A.L. Smit et al. (ed.) Root methods: A handbook. Springer-Verlag, Berlin.

Clausnitzer, V., and J.W. Hopmans. 1994. Simultaneous modeling of transient three-dimensional root growth and soil water flow. Plant Soil 164:299–314.

Clausnitzer, V., and J.W. Hopmans. 2000. Pore-scale measurements of solute breakthrough using microfocus x-ray computed tomography. Water Resour. Res. 36:2067–2079.

Deinert, M.R., J.-Y. Parlange, T.S. Steenhuis, J. Throop, K. Unlu, and K.B. Cady. 2004. Measurement of fluid contents and wetting front profiles by real-time neutron radiography. J. Hydrol. 290:192–201.

Doussan, C., L. Pages, and G. Vercambre. 1998a. Modeling of the hydraulic architecture of root systems: An integrated approach to water absorption: Model description. Ann. Bot. 81:213–223.

Doussan, C., L. Pages, and G. Vercambre. 1998b. Modeling of the hydraulic architecture of root systems: An integrated approach to water absorption: Distribution of axial and radial conductances in maize. Ann. Bot. 81:225–232.

Fortner Research. 1996. Slicer 3D, Version 1.1. Fortner Research, Sterling, VA.

Furukawa, J., T.M. Nakanishi, and M. Matsubayashi. 1999. Neutron radiography of a root growing in soil with vanadium. Nucl. Instrum. Methods Phys. Res. Sect. A 424:116–121.

Garber, D.I., and R.R. Kinsey. 1976. Neutron cross sections. Vol. II: Curves. p. 1–44. Brookhaven Natl. Lab., Upton, NY.

Gibbons, M., and K. Shields. 1998. Preprocessing of backprojection images in the McClellan Nuclear Radiation Center tomography system. Pap. NCT5. McClellan Nuclear Radiation Ctr., Univ. of California, Davis.

Hainsworth, J.M., and L.A.G. Aylmore. 1986. Water extraction by a single plant root. Soil Sci. Soc. Am. J. 50:841–848.

Hassanein, R.K. 2006. Correction methods for the quantitative evaluation of thermal neutron tomography. Ph.D. diss. ETH no. 29045. Swiss Federal Inst. of Technology, Zurich.

Heeraman, D.A., J.W. Hopmans, and V. Clausnitzer. 1997. Three-dimensional imaging of plant roots in situ with x-ray computed tomography. Plant Soil 183:167–179.

Hopmans, J.W., and K.L. Bristow. 2002. Current capabilities and future needs of root water and nutrient uptake modeling. Adv. Agron. 77:104–175.

Hopmans, J.W., T. Vogel, and P.D. Koblik. 1992. X-ray tomography of soil water distribution in one-step outflow experiments. Soil Sci. Soc. Am. J. 56:355–362.

Kak, A., and M. Slaney. 2001. Principles of computerized tomographic imaging. Soc. for Ind. and Appl. Math., Philadelphia.

Koerner, S., B. Schillligner, P. Vontobel, and H. Rauch. 2001. A neutron tomography facility at a low power research reactor. Nucl. Instrum. Methods Phys. Res. Sect. A 471:69–74.

Korosi, F., M. Balasck, and E. Svab. 1999. A distribution pattern of cadmium, gadolinium and samarium in *Phaseolus vulgaris* (L.) plants as assessed by dynamic neutron radiography. Nucl. Instrum. Methods Phys. Res. Sect. A 424:129–135.

Lamarsh, J.R. 1983. Introduction to nuclear engineering. 2nd ed. Addison-Wesley Publ. Co., Reading, MA.

Lilley, J.S. 2001. Nuclear physics: Principles and applications. John Wiley & Sons, Chichester, UK.

Phogat, V.K., and L.A.G. Aylmore. 1999. Evaluation of soil structure by using computer assisted tomography. Aust. J. Soil Res. 27:313–323.

Pierret, A., C. Doussan, and E. Carrigues. 2003. Observing plant roots in their environment: Current imaging options and specific contribution of two-dimensional approaches. Agronomie 23:471–479.

Research Reactor Safety Analysis Services. 1991. McClellan Nuclear Radiation Center safety analysis report. Revision 4. Research Reactor Safety Analysis Services, Kennewick, WA.

Richards, W.J., M.R. Gibbons, and K.C. Shields. 2004. Neutron tomography developments and applications. Appl. Radiat. Isot. 61:551–559.

Schillinger, B., E. Lehmann, and P. Vontobel. 2000. 3D neutron computed tomography: Requirements and applications. Physica B 276–278:59–62.

Sharp, R.E., W.K. Silk, and T.C. Hsiao. 1988. Growth of the maize primary root at low water potentials: I. Spatial distribution of expansive growth. Plant Physiol. 87:50–57.

Silk, W.K., and K.K. Wagner. 1980. Growth-sustaining water potential distributions in the primary corn root. Plant Physiol. 66:859–863.

Solymar, M., E. Leymann, P. Vontaobel, and A. Nordlund. 2003. Relating variations in water saturation of a sandstone sample to pore geometry by neutron tomography and image analysis of thin sections. Bull. Eng. Geol. Environ. 62:85–88.

Somma, F., J.W. Hopmans, and V. Clausnitzer. 1998. Transient three-dimensional modeling of soil water and solute transport with simultaneous root growth, root water and nutrient uptake. Plant Soil 202:281–293.

Tuli, A., and J.W. Hopmans. 2004. Effect of degree of fluid saturation on transport coefficients in disturbed soils. Eur. J. Soil Sci. 55:147–164.

VanDalen, J., C. Logan, and D. Schneberk. 2005. Recent neutron images from MNRC Bay 3. Internal Rep. McClellan Nucl. Radiation Ctr., McClellan, CA.

Vrugt, J.A., J.W. Hopmans, and J. Simunek. 2001. Calibration of a two-dimensional root water uptake model. Soil Sci. Soc. Am. J. 65:1027–1037.

Wildenschild, D., J.W. Hopmans, M.L. Rivers, and A.J.R. Kent. 2005. Quantitative analysis of flow processes in a sand using synchrotron x-ray microtomography. Vadose Zone J. 4:112–126.

Wildenschild, D., J.W. Hopmans, C.M.P. Vaz, M.L. Rivers, D. Rikard, and B.S.B. Christensen. 2002. Using x-ray computed tomography in hydrology: Systems, resolutions, and limitations. J. Hydrol. 267:285–297.

Wilding, M., C.E. Lesher, and K. Shields. 2005. Applications of neutron computed tomography in the geosciences. Nucl. Instr. Methods Phys. Res. Sect. A 542:290–295.